Research Article
doi.org/10.1002/cplu.202300234

Chemistry Europe
European Chemical Societies Publishing

www.chempluschem.org

Special Collection

Silver and Gold Pillarplex Pseudorotaxanes from α,ω-Dicarboxylic Acids

Alexandra A. Heidecker,[a] Michele Stasi,[b] Alexander Spears,[a] Job Boekhoven,[b] and Alexander Pöthig*[a]

A series of pseudorotaxanes with supramolecular organometallic silver(I) and gold(I) pillarplexes acting as rings and different α,ω-dicarboxylic acids as axle components are reported. The successful formation of the host-guest complexes is shown by ^{1}H NMR spectroscopy and respective NMR titration. Additional evaluation with ITC titration experiments yielded dissociation constants (K_d) ranging from 10^{-5} to 10^{-7} M. Single-crystal X-Ray diffraction analysis reveals a particularly exciting pore alignment of different examples in the solid state depending on the length of the guest. The work highlights, that dicarboxylic acids can penetrate the tight tubular pillarplex pore, paving the way to future mechanically interlocked molecules and materials.

Introduction

Organic macrocycles, such as cyclodextrins,[1] cucurbit[n]urils,[2] or pillar[n]arenes,[3] are prominently used as host molecules in supramolecular chemistry. They can also be employed as ring components in rotaxanes, i.e., mechanically interlocked architectures.[4–7] However, their oligomeric composition leads to defined pore sizes, which can only be changed in discrete steps of monomer units.[8]

Therefore, a finer tuning of the pore size is impossible. For example, the smallest congeners of cucurbit[n]uril – cucurbit[5]uril (Figure 1A) – only allows the encapsulation of small molecules such as dinitrogen or dioxygen due to their very narrow pore opening (2.4 Å).[2] In contrast, the pore of the smallest pillar[5]arene (4.7 Å, Figure 1C),[9] as well as the larger cucurbit[6]uril,[2] already allow for the uptake of linear and functionalised hydrocarbons and/or larger aromatic compounds.[10–12]

In 2016, we introduced the pillarplexes $[M_8L_2](X)_4$[13–14] (Figure 1B) using macrocyclic hybrid imidazole/pyrazole cyclophane cyclophanes[15] to be metalated with Ag(I) or Au(I) coinage metal ions and are examples of supramolecular organometallic complexes (SOCs).[16–17] In general there are only a handful examples of SOCs, most of which are NHC based and have been reported in the last years, e.g. by Hahn, Peris and Han.[17–22] In contrast to many other SOCs, the pillarplexes can also act as metallocavitands[23] since they feature a tubular pore and show tuneable solubility, induced pore flexibility,[24] as well as intrinsic luminescence for the gold(I) congeners. A similar strategy has been implemented by Sue et al. using functionalised pillararenes to form metal-organic pillars very recently.[25] Significantly, for the pillarplex, the size of the macrocyclic ligand determines the size of the resulting pore with an inner diameter of 4.3 Å (Figure 1B) – located in between cucurbit[5]uril and pillar[5]arene – enabling a shape-selective guest encapsulation of linear molecules over aromatic compounds. This was previously studied by the encapsulation of sterically undemanding diamino alkanes, and their host-guest complex behaviour and occurring interactions were investigated (see Figure 2B).[13,26] Based on these experiments the key factors controlling the guest encapsulation into the pillarplex cavity are hydrophobic interactions and the tubular shape of the respective cavity. The encapsulated diamino alkanes can be further converted to pillarplex [2]rotaxanes by introducing bulky stopper motifs.[14]

[a] A. A. Heidecker, A. Spears, Dr. A. Pöthig
Technical University of Munich
TUM School of Natural Sciences, Department of Chemistry
Chair of Inorganic and Metal-Organic Chemistry; Catalysis Research Center (CRC)
Ernst-Otto-Fischer-Straße 1
85748 Garching, (Germany)
E-mail: alexander.poethig@tum.de
[b] M. Stasi, Prof. Dr. J. Boekhoven
Technical University of Munich
TUM School of Natural Sciences, Department of Chemistry
Chair of Supramolecular Chemistry
Lichtenbergstraße 4
85748 Garching, (Germany)

Supporting information for this article is available on the WWW under https://doi.org/10.1002/cplu.202300234

Part of a Special Collection on Gold Chemistry

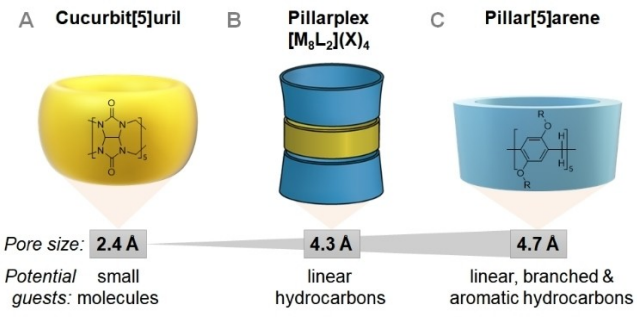

Figure 1. Schematic representation of the structure of smallest congeners of tubular cavitand families. (A) cucurbit[5]uril, (B) pillarplex and (C) pillar[5]arene showing the increasing size of the pore opening.

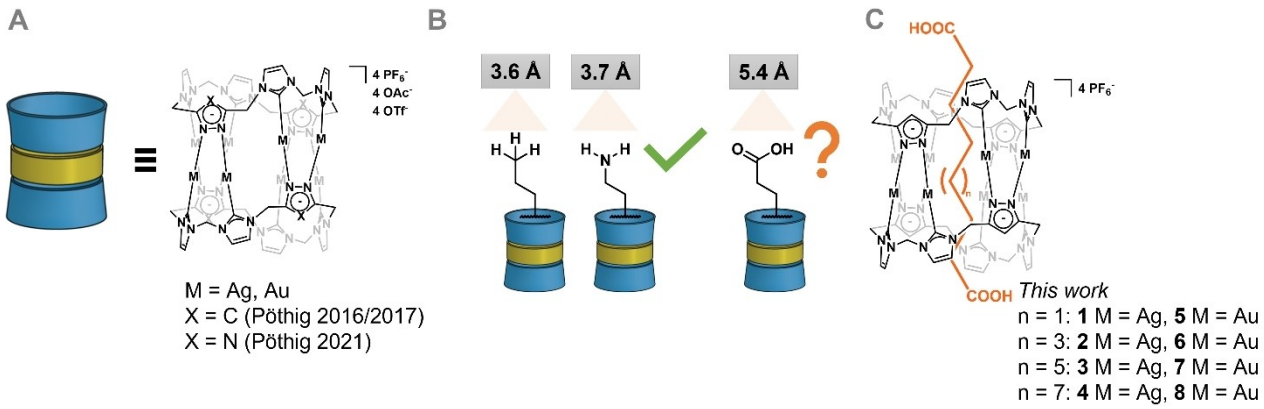

Figure 2. (A) Structural formula of the pillarplex salts; (B) Comparison of the diameter of (potential) guest molecules containing terminal $-CH_3$, $-NH_2$ and –COOH groups to be encapsualted into the pillarplex pore; (C) General composition of pillarplex pseudorotaxanes formed by encapsulation of linear α,ω-dicarboxylic acids (this work).

We now became interested if the steric demand of α,ω-functionalised linear guests could be increased and incorporation into the tubular pillarplex pores would still be observed. As the target guest molecule, carboxylic acids as terminal functional groups were chosen, since they are highly interesting for the subsequent build-up of mechanically interlocked molecules or materials. At the same time the central alkyl chains of the guests match with the hydrophobic confinement inside the pillarplex cavity. Simultaneously, they have a larger steric demand than the previously incorporated guests. Assuming a static cavity of the host system (i.e., no ligand dissociation or breathing), the carboxylic acid group should already be sterically too demanding opening of the pillarplex. Typically, SOCs show static behaviour as they feature strong organometallic bonds. Therefore the inclusion of guests is expected only upon conformational changes, e.g. breathing effects.[16] If a dissociation occurs to allow guest encapsulation, the Ag(I) congeners are more likely to show this behaviour than the Au(I) ones due to different bond strengths.[27]

Results and Discussion

To investigate the encapsulation of dicarboxylic acids into pillarplexes, we attempted to synthesise a series of pseudorotaxanes with various dicarboxylic acids as guest molecules (Figure 2C). The pillarplex salt $[M_8L^{Me}_2][PF_6)_4$ was treated with the respective dicarboxylic acid $C_nH_{2n-2}O_4$ (M = Ag, n = 8 (**1**), 10 (**2**), 12 (**3**), 14 (**4**); M = Au, n = 8 (**5**), 10 (**6**), 12 (**7**), 14 (**8**)) in acetonitrile (MeCN) and stirred at room temperature for 10 min. The dicarboxylic acids themselves show limited solubility in MeCN (ca. 1 g L^{-1}), but due to the strong hydrophobic interactions with the pillarplex cavity as driving force for the formation of a host-guest system, a relatively fast dissolution of the guest molecules was observed. In dimethyl sulfoxide (DMSO) a significantly higher solubility of the dicarboxylic acids was observed (ca. 1000 g L^{-1}). After removal of the solvent, pseudorotaxanes $[M_8L^{Me}_2](C_nH_{2n-2}O_4)(PF_6)_4$ were successfully isolated as white solids. The formation of **1**–**8** was experimentally validated by NMR spectroscopy (^1H,^{13}C,^{31}P) (Figure 1S–40S) and the product formation was additionally characterised by IR spectroscopy indicating the combined bands of host and guest systems (Figure 73S–80S) and elemental analysis. In ^1H NMR spectra, upon guest encapsulation into the pore an upfield shift of the alkyl proton signals of the guest is expected due to shielding effects, which experimentally was confirmed by ^1H NMR spectroscopy for all pseudorotaxanes in acetonitrile (MeCN-d_3). To further corroborate specific guest binding inside the pore, 2D NMR experiments of **1**–**8** were performed in MeCN-d_3. While the DOSY spectra support the formation of only one existing species indicating only specific interactions (Figure 41S–48S), the NOESY spectra showed no cross-signals between the host and guest. Only the expected cross-signal of the pillarplex protons and the cross-signals of the guest protons themselves were observed (Figure 49S–56S). NMR experiments (^1H, DOSY, NOESY) were repeated in DMSO-d_6. Interestingly, in DMSO-d_6, the ^1H NMR spectra of **1**–**8** confirmed the protonation of the dicarboxylic acids with signals visible in the range of 11.34–11.92 ppm (Figure 9S–16S) for the acidic proton. In contrast, these signals were not visible in the ^1H NMR spectra measured in MeCN-d_3. In the case of **3** and **4**, the host-guest formation was also confirmed by the respective cross-signals between the protons of the guest and the host in the NOESY spectra in DMSO-d_6 (Figure 59S–60S).

To evaluate the thermal stability and the dissociation of the host-guest complexes, variable temperature NMR spectroscopy (in DMSO-d_6) was performed in 20 °C steps. The full set of signals for pseudorotaxanes **1**, **5** and **6** were found up to 40 °C and for **2**, **3**, **4**, **7** and **8** up to 60 °C (Figure 65S–72S), while the guest proton signals are broadened and shifted towards higher ppm values at elevated temperatures. Consequently, a temperature-dependent dynamic equilibrium of encapsulated and non-encapsulated guest molecules can be expected, indicating that the dicarboxylic acids are located outside the cavity to a higher degree at elevated temperatures. Interestingly, the pillarplex signals remain unchanged at higher temperatures showing that the host system itself has a high thermal stability.

The absorption maxima of **1**–**8** were investigated by UV-vis spectroscopy in solution and in the solid-state, where absorption maxima in the range of 240–270 nm for Ag(I) congeners **1**–**4** and in the field of 230–340 nm for the Au(I) pseudorotaxanes **5**–**8** (Figure 81S–84S) were found. The Au(I) congeners **5**–**8** were also tested towards their emission and luminescence properties. As already theoretically rationalised by destabilising the excited state of $[Au_8L^{Me}{}_2](PF_6)_4$ upon guest incorporation, no emission in solution was detected.[28] But in the solid state, **5**–**8** exhibit hypsochromic shifted maxima ($\lambda_{ex}=315$–325 nm, $\lambda_{max}=394$–402 nm) in comparison to the "empty $[Au_8L^{Me}{}_2](PF_6)_4$ pillarplex with $\lambda_{ex}=335$ nm and absorption maximum of $\lambda_{max}=430$ nm[13] (Figure 85S–88S).

Titration experiments

^{1}H NMR titration experiments of the four dicarboxylic acids to $[M_8L^{Me}{}_2](PF_6)_4$ were conducted to determine the binding constant and the stoichiometry of host-guest interaction. For this, a solution of $C_nH_{2n-2}O_4$ was prepared and aliquots of $[M_8L^{Me}{}_2](PF_6)_4$ were added. Exemplary in Figure 3, the titration of $[Ag_8L^{Me}{}_2](PF_6)_4$ with $C_8H_{12}O_4$ in MeCN-d_3 is shown. For all titrations, continuous upfield shifting of the guest proton signals can be seen supporting a fast equilibrium of host-guest complex formation concerning the time scale of the NMR experiment (Figure 99S–106S). As the shifting of the guest proton signals was visible for **1**–**6**, these ^{1}H NMR titrations were used to calculate binding constants K_d for host-guest complexes ranging from 0.0019–$1.99\cdot10^{-3}$ M (Table 1S) or from 3. $\cdot10^{-3}$ to 2.147 10^{-6} (Table 1S). As in all titrations, several proton signals could be assigned, the performance of a Job Plot titration analysis was possible and supports a stoichiometry of 1 : 1 for all host-guest complexes (Figure 107S-114S). NMR titrations were repeated in DMSO-d_6, which showed also fast equilibria for titrations of $C_8H_{12}O_4$ to $[M_8L^{Me}{}_2](PF_6)_4$ and $C_{10}H_{18}O_4$ to $[Ag_8L^{Me}{}_2](PF_6)_4$. The titrations of $C_{10}H_{18}O_4$ to $[Au_8L^{Me}{}_2](PF_6)_4$, $C_{12}H_{22}O_4$ to $[M_8L^{Me}{}_2](PF_6)_4$ and $C_{14}H_{26}O_4$ to $[M_8L^{Me}{}_2](PF_6)_4$ showed the formation of two species indicating a slow equilibrium (Figure 123S, 124S, 126S–128S) yielding binding constants of K_d for host-guest complexes **3**, **4**, **6**–**8** of 2.63–$8.97\cdot10^{-5}$ M (Table 5S). Here, a second set of pillarplex proton signals (in the range of 9–5 ppm) is visible upon the addition of more than 1.0 eq. of $[M_8L^{Me}{}_2](PF_6)_4$ indicating the simultaneous presence of occupied and empty host above a host-guest stoichiometry of 1 : 1. With this behaviour of a rather slow equilibrium, already after the addition of 0.2 eq. of guest the respective guest proton signals are upfield shifted and during further addition of guest no shifting is observed. Unfortunately, this hinders the determination of the corresponding binding constants and the determination of stoichiometry. Nevertheless, we observed the high dependency of respective host-guest complexes towards the applied solvent (MeCN vs. DMSO). Interestingly, the mode of host-guest interaction is also strongly dependent on the alkyl chain length of the guest (fast exchange for short acid vs. slow exchange for longer acids) as observed in similar tubular deep-cavitand systems very recently.[29]

To gain further insights into the different behaviours of the host-guest binding equilibria in MeCN, we performed Isothermal Calorimetry (ITC) experiments. ITC relies on heat changes due to the chemical events under investigation only and therefore is not dependent on the choice of signals as we observed in the ^{1}H NMR titration experiments. Each pillarplex $[M_8L^{Me}{}_2][PF_6)_4$ in acetonitrile was titrated with the appropriate dicarboxylic acid to form the pseudorotaxane. A binding isotherm was used to fit the raw heat released at each addition of guest and extract thermodynamic information.

All complexes show a strong enthalpic-driven force, consistent with the formation of non-covalent interaction of the linear alkyl chain with the inner cavity of the pillarplex. Similarly, an entropic penalty (see Table 1) can be observed for all the

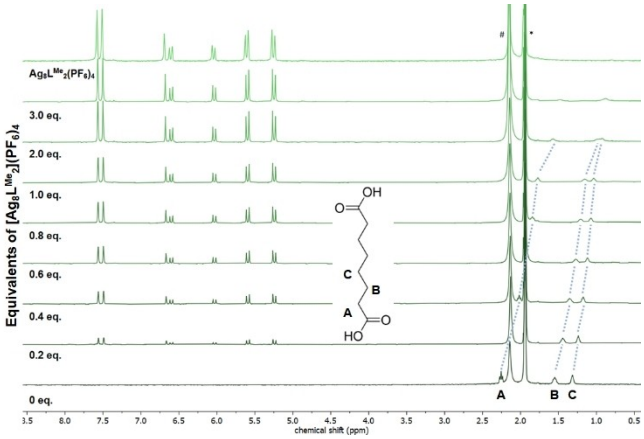

Figure 3. ^{1}H NMR titration (400 MHz, 298 K) of a 2.85 mM solution of $[Ag_8L^{Me}{}_2](PF_6)_4$ in MeCN-d_3 into a 1.43 mM solution of $C_8H_{12}O_4$ in MeCN-d_3. Signals marked with * are assigned to MeCN (1.94 ppm) and # are assigned to water (2.13 ppm). The signals between 5 and 8 ppm are assigned to $[Ag_8L^{Me}{}_2](PF_6)_4$. Due to electronic shielding of the guest molecule inside the cavity, the proton signals of 1,8-octane diacid are upfield shifted and their assignment was verified by 2D-COSY NMR spectroscopy. A binding constant K_d of $1.99\pm0.70\cdot10^{-3}$ M was calculated.

Table 1. Results of the ITC titration experiments including the change of enthalpy (ΔH), entropy (TΔS), determined binding constants K_d and the calculated number of sites (N).

	Dicarboxylic Acid	ΔH (kcal/mol)	TΔS (kcal/mol)	K_d (M)	N number of sites
Ag	$C_8H_{14}O_4$	−10.8 ± 2.8	−3.53	4.8e-6 ± 4.9e-7	1.09 ± 0.21
	$C_{10}H_{18}O_4$	−14.8 ± 0.48	−7.67	5.75e-6 ± 4.6e-7	0.604 ± 0.013
	$C_{12}H_{22}O_4$	−23.3 ± 0.85	−16.2	6.12e-6 ± 3.3e-7	0.351 ± 0.010
	$C_{14}H_{26}O_4$	−21.8 ± 0.45	−14.1	2.01e-6 ± 1.2e-7	0.354 ± 0.005
Au	$C_8H_{14}O_4$	−17.9 ± 3.54	−10.9	7.77e-6 ± 3.09e-6	1.02 ± 0.16
	$C_{10}H_{18}O_4$	−28.9 ± 6.92	−22.4	1.63e-5 ± 7.4e-6	1.06 ± 0.19
	$C_{12}H_{22}O_4$	−25.3 ± 1.42	−17.6	2.29e-6 ± 3.9e-7	0.394 ± 0.010
	$C_{14}H_{26}O_4$	−33.6 ± 0.41	−25.3	8.50e-7 ± 4.6e-8	0.312 ± 0.002

samples, with an increase in magnitude going from $C_8H_{14}O_4$ to $C_{14}H_{26}O_4$. The co-localisation due to the formation of the inclusion complex, coupled with the reduction of conformational freedom of the alkyl chain is the main responsible for the decrease of entropy in the system. The K_d determined from ITC experiments are in the range of μM for all tested dicarboxylic acids and consistent with the similar structure of the substrates and interaction involved. These values strongly differ from the ones derived from . Here, it should be noted that ITC uses a quadratic equation to fit the binding isotherm making it independent from the assumption of a constant concentration of free ligand. It also operates in a concentration range close to the K_d value, which is a condition to avoid the "titration regime" and overestimate the K_d value.[30]

Interestingly, the ITC-derived binding stoichiometry (i.e., the number of sites) for the long-chain carboxylic acid differs from the expected 1:1 ratio. Both pillarplexes show approximately a 3:1 stoichiometry with the $C_{12}H_{22}O_4$ and $C_{14}H_{26}O_4$ dicarboxylic acid, indicating that more than one pillarplex could slide along the axle. This is also reflected by the higher enthalpy and entropy changes measured for $C_{14}H_{26}O_4$ vs $C_8H_{14}O_4$. This exciting behaviour was not observed before, but the length of the diacids $C_{12}H_{22}O_4$ and $C_{14}H_{26}O_4$ entails the possibility of non-covalent interactions between the acid group and pillarplex rim, which can lead to the stoichiometry of 3:1. However, comparing the calculated stoichiometries from ITC and ^{1}H NMR titration experiments, indicates a strong dependency of the obtained host-guest complexes and the concentration.

Crystallographic Analysis

Single crystals suitable for single crystal X-Ray diffraction were obtained by slow evaporation of tetrahydrofuran (THF) into a saturated solution of **2**–**4** in acetonitrile. Colourless crystals of **2** were solved and refined in the monoclinic space group *C*2 (No. 5) featuring half of a $[Ag_8L^{Me}{}_2]^{4+}$ cation, two PF_6^- anions disordered on different positions, as well as two THF molecules in the asymmetric unit. **3** was obtained as plate-like colourless crystals and the structure was solved and refined in monoclinic space group *I*2 (No. 5). Here, the asymmetric unit contains two and a half pillarplex cations, nine PF_6^- anions and 13 THF molecules. The colourless, plate-shaped crystals of **4** were refined in the space group triclinic *P*1 (No. 2) with the asymmetric unit containing two $[Ag_8L^{Me}{}_2]^{4+}$ cations, nine PF_6^- anions and 12 THF molecules (for detailed crystallographic data see sections 3.1–3.4 in the Supporting Information). Unfortunately, a high disorder of the guest molecules inside the cavity was observed and thus we were not able to refine them explicitly. Therefore, PLATON/SQUEEZE[31] procedure was performed. To verify the presence of guest molecules inside the cavity, the number of squeezed electrons inside the cavities of **2**–**4** was evaluated towards the expected guests. Besides disordered acetonitrile molecules pointing towards the methylene groups of $[Ag_8L^{Me}{}_2]^{4+}$, two $C_{10}H_{18}O_4$ molecules (110 e^- per molecule) were squeezed in the unit cell of **2**. In the unit cell of **3** a total of 876 e^- were squeezed approximately matching the ten molecules $C_{12}H_{22}O_4$ (126 e^-). The 579 e^- squeezed in the unit cell of **4** correspond to the four guest molecules (142 e^-/$C_{14}H_{26}O_4$). These findings verify the successful encapsulation of the α,ω-diacids into the pillarplex pore both in liquid and solid state.

The carboxylic groups additionally inherit high potential to form non-covalent interactions, especially hydrogen bonding, hence, the crystal packing in the solid state was evaluated in greater detail (Figure 4). As the incorporated diacid molecules could not be refined explicitly, the removed electron density has been visualised as void volume (1.2 Å) by Mercury. [32] In the case of **2** isolated $[Ag_8L^{Me}{}_2]^{4+}$ cations are observed with the voids of the potential guest molecules being completely enclosed inside of the pillarplex cavity. Hereby, the rim (cf. Figure 5A) forms non-covalent interactions with PF_6^- and THF molecules. This can be visualised by Hirshfeld surface analysis[33] for which the interactions of $[Ag_8L^{Me}{}_2]^{4+}$ with THF molecules are depicted in Figure 5B. The THF molecules are located on top of the cavity blocking the pore opening. Similarly, non-classical hydrogen bonding of the rim with PF_6^- anions is also present (see section 3, Supporting Information), which has already been previously observed for pillarplexes.[24] However, for **3** and **4** a pore alignment of the $[Ag_8L^{Me}{}_2]^{4+}$ cations can be observed along the *c*-axis (**3**) or the *a*-axis (**4**), respectively (Figure 4B&C). Hereby, no PF_6^- anions or THF molecules are found in proximity of the rim for **3** or **4**, instead these molecules are only located lateral to the $[Ag_8L^{Me}{}_2]^{4+}$ cations. Consequently, for **3** and **4** Hirshfeld surface analysis (Figure 5B&C) shows mainly interactions with the methylene bridge or metal ions but not with the rim of the pillarplex cations.

Closer inspection of the pore cavities shows that in the case of **2** the respective void volume (Figure 4A, depicted in brown) is exclusively present inside the pillarplex cations corresponding to the electron density of the guest molecules. This corresponds to a complete encapsulation of the guest and is in accordance with the crystal packing, where no significant influence of the guest towards the packing of the $[Ag_8L^{Me}{}_2]^{4+}$ cations is visible. In contrast, for **3** and **4** the pore voids form quasi-continuous channels connecting the pore-aligned neighbouring pillarplex cations (Figure B&C, depicted in brown). This is likely explained by the fact that the incorporated diacids are longer than the diacid encapsulated in **2**, now presenting the carboxylic groups outside the cavities. Hereby, hydrogen bonding with the rim of neighbouring pillarplex cations, which already was observed for the pillarplexes with, e.g. counter anion PF_6^- and solvent molecules, or hydrogen bonding between two neighbouring acids is enabled.[24,26] By inspecting the Hirshfeld surface analysis of **3** and **4**, mainly potential hydrogen bonding sites at the rim are observed, therefore **3** and **4** resemble hydrogen-bonded polypseudorotaxanes[34–35] in the solid state. These new findings, that the variation of guest molecules to encapsulate into pillarplexes can strongly influence the packing and the occurring (non–)covalent interactions, makes those mechanically-interlocked molecules interesting in the context of recently introduced hydrogen-bonded frameworks (HOFs)[36–39] and in the context of crystal engineering.[40]

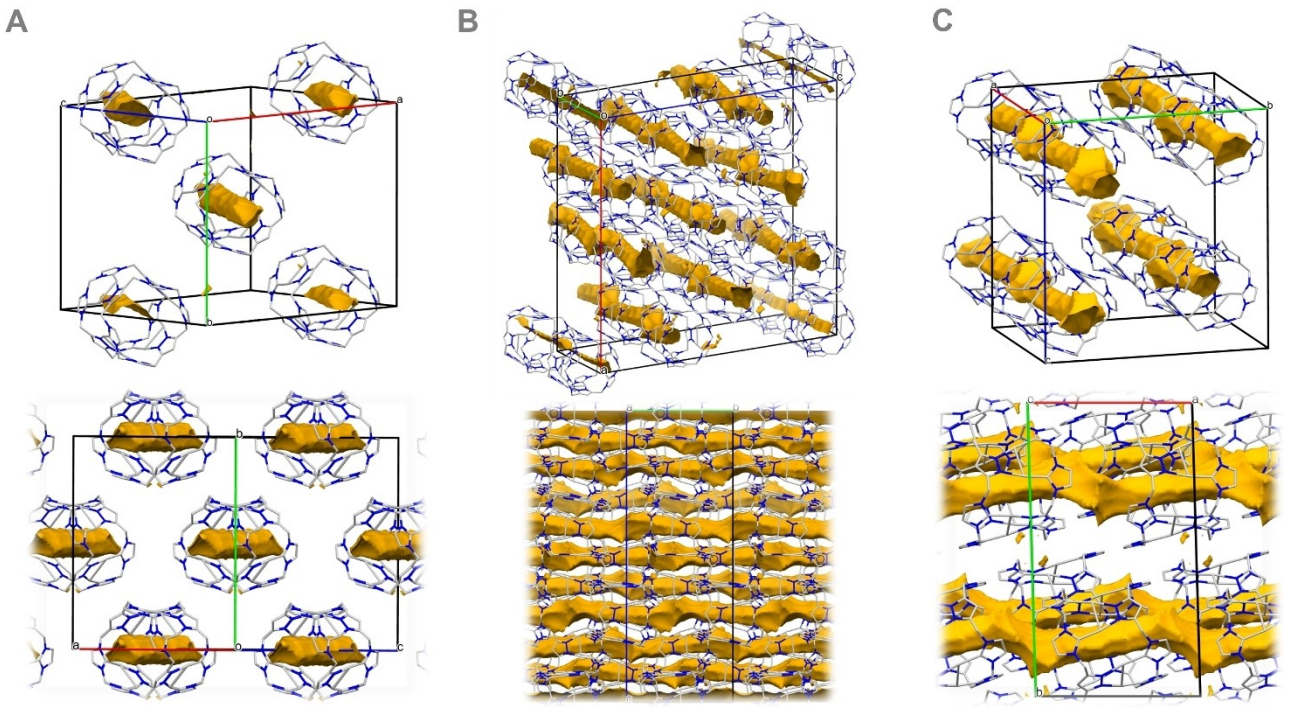

Figure 4. Crystal packing of cations $[Ag_8L^{Me}_2]^{4+}$ with the visualisation of the intra-pore solvent accessible surface (brown, probe radius of 1. Å: (A) Pore cavity in **2** showing separated, non-connected voids, (B) Connected voids in **3** showing pore-alignment along the crystallographic c-axis and (C) connected voids in **4** showing pore alignment along the crystallographic a-axis. Note: The incorporated dicarboxylic acid guest molecules could not be explicitly refined and were treated using the PLATON/SQUEEZE procedure.

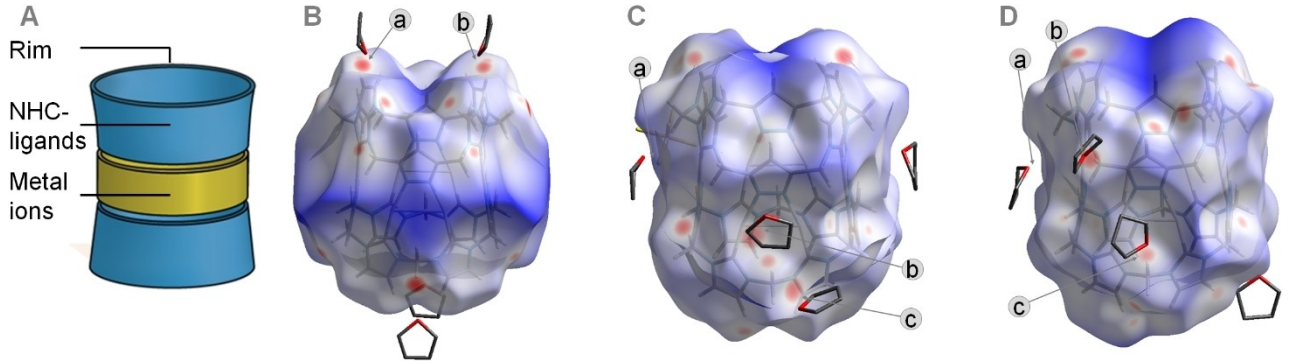

Figure 5. (A) Regions of pillarplex cation for potential non-covalent interactions. Hirshfeld surface analysis of pillarplex cation $[Ag_8L^{Me}_2]^{4+}$ in the solid state showing short intermolecular contacts (red) with corresponding donor-acceptor [Y•••Z] distances: (B) for **2** with classical hydrogen bonding **a** O···H 2.445 Å and 2.454 Å, **b** O···H 2.479 Å and 2.511 Å; (C) for **3** with classical hydrogen bonding **a** O···H 3.641 Å, **b** O···H 3.134 Å, **c** O···H 2.788 Å; (D) for **4** with classical hydrogen bonding **a** O···H 3.202 Å, **b** O···H 2.468 Å, **c** O···H 2.685 Å. Note: Surface areas in blue (pores and at metal ions in B) originate from SQUEEZE procedure.

Conclusions

In summary, the results support the successful guest uptake of the dicarboxylic acids into the pillarplex cavity to form the corresponding pseudorotaxanes. This proves a certain (conformational) flexibility of Ag- and Au-pillarplexes, allowing guest uptake. The host-guest formation is governed by the complementarity of the guest molecules (linear shape, hydrophobic central chain, chain length) and the pillarplex pore (tubular shape, hydrophobic pore) going along with a potential solvophobic effect in MeCN. This is supported by ITC measurements in MeCN, showing the encapsulation being enthalpy-driven. The pseudorotaxanes' crystal packing was highly dependent on the length of the axle molecules, most likely due to different possible hydrogen bonding interactions forming polypseudorotaxanes in the solid state. These results pave the way to implement pillarplex-dicarboxylic acid pseudorotaxanes as building blocks into future supramolecular or mechanically interlocked materials.

Experimental Section

General Synthesis of pseudorotaxanes $[M_8L^{Me}_2](Diacid)(PF_6)_4$ (1-8). $[M_8L^{Me}_2](PF_6)_4$ (1 eq.) and $C_nH_{2n-2}O_4$ (1.1 eq.) were dissolved in acetonitrile and the mixture was stirred at room temperature for 10 min. The solvent was removed *in vacuo* at room temperature and a white solid was obtained.

NMR spectra were recorded on NMR spectrometer *Bruker* AV400US, *Bruker* AVHD400, and *Bruker* AV500C at 298 K. The spectra were referenced to the residual solvent shift as internal standard (MeCN-d_3, ^{1}H NMR $\delta = 1.94$ ppm, ^{13}CNMR $\delta = 118.26$ ppm; DMSO-d_6, ^{1}H NMR $\delta = 2.50$ ppm, ^{13}C NMR $\delta = 39.51$ ppm).

NMR titration. To a 1.425 mM solution of guest ($C_8H_{14}O_4$, $C_{10}H_{16}O_4$, $C_{12}H_{22}O_4$, $C_{14}H_{26}O_4$) in MeCN-d_3 or DMSO-d_6 a 2.850 mM solution of $[M_8L^{Me}_2](PF_6)_4$ in MeCN-d_3 or DMSO-d_6 was added and ^{1}H NMR spectroscopy was performed. Analysis of the ^{1}H NMR titration data was performed by DynaFit,[41] Job Plot, BindFit[42–43] for a fast host-guest exchange (in MeCN-d_3) or the integral ratio of free and encapsulated guest signals for a slow host-guest exchange (in DMSO-d_6).

ITC titrations. Isothermal titration experiments were performed on a MicroCal PEAQ-ITC from Malvern Pananalytical. All experiments were performed at 25 °C in pure acetonitrile. The reference cell was filled with acetonitrile. For all the titrations the following conditions were used: sample cell was filled with either $[Au_8L^{Me}_2](PF_6)_4$ or $[Ag_8L^{Me}_2](PF_6)_4$ to a final concentration of 30 μM. The dicarboxylic acid was loaded in the titration syringe to a concentration of 200 μM. Titration was performed with 1 injection of 0.4 μL followed by 18 injections of 2 μL. Injection duration was set to 4 s, spacing between injection 150 s and stirring speed to 750 rpm to ensure homogeneous mixing of the solution. For each dicarboxylic acid a control titration versus acetonitrile was performed and used to correct heat of dilution. Data were fitted using a non-linear least squares regression algorithm provided with the Malvern PEAQ-ITC Analysis Software. For all titration, a "one-set of site" binding isotherm was used. Errors correspond to error of the fit.

Single crystal X-ray diffraction data were collected on a Bruker D8 Venture diffractometer equipped with a CMOS detector (Bruker Photon-100), a TXS rotating anode with MoK_α ($\lambda = 0.71073$ Å) and a Helios mirror optic using the software package APEX3 and APEX4.[45] Measurements were performed on a single crystal coated with perfluorinated ether and the crystal was fixed on top of a Kapton micro sampler, transferred to the diffractometer and frozen under a stream of cold nitrogen. A matrix scan was used to determine the initial lattice parameters. Reflections were merged and corrected for Lorenz and polarisation effects, scan speed and background using SAINT.[46] Absorption corrections, including odd and even ordered spherical harmonics were performed using SADABS.[46] Based on systematic absences, E-statistics, and successful refinement of the structures, the space group was assigned. The structure was solved by direct methods[47] with aid of successive difference Fourier maps, refined using APEX3 and APEX4 software, in conjugation with SHELXL-2018/3, SHELXL-2019/1 and SHELXLE.[47–49] Hydrogen atoms were calculated in ideal positions with $U_{iso}(H) = 1.2\ U_{eq}(C)$. Non-hydrogen atoms were refined using anisotropic displacement parameters. Full-matrix least-squares refinements were carried out by minimising $\Sigma w(F_o^2 - F_c^2)^2$ with the SHELXL weighting scheme.[49] Neutral atom scattering factors for all atoms and anomalous dispersion corrections for the non-hydrogen atoms were taken from *International Tables for Crystallography*.[50]

Disordered molecule, which was treated as a diffused contribution to the overall scattering without specific atom positions using the PLATON/SQUEEZE procedure.[51] Images of the crystal structure were generated with MERCURY and PLATON.21.[52–53]

Supporting Information

Additional references cited within the Supporting Information.[13,15, 31–33,41–56] Deposition Numbers 2196097 (for **3**), 2196098 (for **4**) and 2196099 (for **2**) contain the supplementary crystallographic data for this paper. These data are provided free of charge by the joint Cambridge Crystallographic Data Centre and Fachinformationszentrum Karlsruhe Access Structures service.

Acknowledgements

AAH and AP thank the TUM Catalysis Research Center, TUM School of Natural Sciences (Chemistry), the TUM Graduate School and the Deutsche Forschungsgemeinschaft (DFG SPP1928 – 434509373) for the funding of this work. ITC measurements are funded by the Deutsche Forschungsgemeinschaft (DFG) under Germany's Excellence Strategy – EXC-2094 – 390783311. M.S and J.B. thanks for funding the Max Planck School Matter to Life supported by the German Federal Ministry of Education and Research (BMBF) in collaboration with the Max Planck Society. Open Access funding enabled and organized by Projekt DEAL.

Conflict of Interests

The authors declare no conflict of interest.

Data Availability Statement

The data that support the findings of this study are available in the supplementary material of this article.

Keywords: host-guest systems · organometallic chemistry · pillarplexes · pseudorotaxanes · supramolecular · chemistry

[1] E. M. M. Del Valle, *Process Biochem.* **2004**, *39*, 1033–1046.
[2] J. Lagona, P. Mukhopadhyay, S. Chakrabarti, L. Isaacs, *Angew. Chem. Int. Ed.* **2005**, *44*, 4844–4870.
[3] M. Xue, Y. Yang, X. Chi, Z. Zhang, F. Huang, *Acc. Chem. Res.* **2012**, *45*, 1294–1308.
[4] S. J. Loeb, *Chem. Commun.* **2005**, 1511–1518.
[5] Q. Li, H. Zhu, F. Huang, *Trends Chem.* **2020**, *2*, 850–864.
[6] K. Yang, S. Chao, F. Zhang, Y. Pei, Z. Pei, *Chem. Commun.* **2019**, *55*, 13198–13210.
[7] H.-W. Schmidt, F. Würthner, *Angew. Chem. Int. Ed.* **2020**, *59*, 8766–8775.
[8] Y. Chao, T. U. Thikekar, W. Fang, R. Chang, J. Xu, N. Ouyang, J. Xu, Y. Gao, M. Guo, H. Zuilhof, A. C.-H. Sue, *Angew. Chem. Int. Ed.* **2022**, *61*, e202204589.
[9] P. J. Cragg, K. Sharma, *Chem. Soc. Rev.* **2012**, *41*, 597–607.
[10] T. Ogoshi, T. Yamagishi, *Chem. Commun.* **2014**, *50*, 4776–4787.
[11] X.-B. Hu, L. Chen, W. Si, Y. Yu, J.-L. Hou, *Chem. Commun.* **2011**, *47*, 4694–4696.
[12] G.-Y. Wu, B.-B. Shi, Q. Lin, H. Li, Y.-M. Zhang, H. Yao, T.-B. Wei, *RSC Adv.* **2015**, *5*, 4958–4963.
[13] P. J. Altmann, A. Pöthig, *J. Am. Chem. Soc.* **2016**, *138*, 13171–13174.
[14] P. J. Altmann, A. Pöthig, *Angew. Chem. Int. Ed.* **2017**, *56*, 15733–15736.
[15] P. J. Altmann, C. Jandl, A. Pöthig, *Dalton Trans.* **2015**, *44*, 11278–11281.
[16] A. Pöthig, A. Casini, *Theranostics* **2019**, *9*, 3150–3169.

[17] S. Ibáñez, M. Poyatos, E. Peris, *Acc. Chem. Res.* **2020**, *53*, 1401–1413.
[18] S. Bai, Y.-F. Han, *Acc. Chem. Res.* **2023**, *56*, 1213–1227.
[19] Y.-S. Wang, H. Li, S. Bai, Y.-Y. Wang, Y.-F. Han, *Science China Chemistry* **2023**, *66*, 778–782.
[20] M.-M. Gan, J.-Q. Liu, L. Zhang, Y.-Y. Wang, F. E. Hahn, Y.-F. Han, *Chem. Rev.* **2018**, *118*, 9587–9641.
[21] S. Rupp, P. D. Dutschke, J. Kinas, A. Hepp, F. Ekkehardt Hahn, *Eur. J. Inorg. Chem.* **2022**, *2022*, e202200216.
[22] K. Hua, X. Li, Y.-F. Han, *J. Organomet. Chem.* **2020**, *917*, 121250.
[23] P. D. Frischmann, M. J. MacLachlan, *Chem. Soc. Rev.* **2013**, *42*, 871–890.
[24] S. Guan, T. Pickl, C. Jandl, L. Schuchmann, X. Zhou, P. J. Altmann, A. Pöthig, *Org. Chem. Front.* **2021**, *8*, 4061–4070.
[25] X. Wan, S. Li, Y. Tian, J. Xu, L.-C. Shen, H. Zuilhof, M. Zhang, A. C.-H. Sue, *Chem* **2022**, *8*, 2136–2147.
[26] A. A. Heidecker, M. Bohn, A. Pöthig, *Z. Kristallogr. - Cryst.* **2022**, *237*, 167–177.
[27] R. C. Nishad, S. Kumar, A. Rit, *Angew. Chem. Int. Ed.* **2022**, *61*, e202206788.
[28] M. Rojas-Poblete, P. L. Rodríguez-Kessler, R. Guajardo Maturana, A. Muñoz-Castro, *Phys. Chem. Chem. Phys.* **2021**, *23*, 15917–15924.
[29] Y. Tian, Y. Guo, X. Dong, X. Wan, K.-H. Cheng, R. Chang, S. Li, X. Cao, Y.-T. Chan, A. C. H. Sue, *Nature Synthesis* **2023**, *2*, 395–402.
[30] I. Jarmoskaite, I. AlSadhan, P. P. Vaidyanathan, D. Herschlag, *eLife* **2020**, *9*, e57264.
[31] A. Spek, *Acta Crystallogr. Sect. C* **2015**, *71*, 9–18.
[32] C. F. Macrae, I. Sovago, S. J. Cottrell, P. T. A. Galek, P. McCabe, E. Pidcock, M. Platings, G. P. Shields, J. S. Stevens, M. Towler, P. A. Wood, *J. Appl. Crystallogr.* **2020**, *53*, 226–235.
[33] P. R. Spackman, M. J. Turner, J. J. McKinnon, S. K. Wolff, D. J. Grimwood, D. Jayatilaka, M. A. Spackman, *J. Appl. Crystallogr.* **2021**, *54*, 1006–1011.
[34] B. M. Rambo, H.-Y. Gong, M. Oh, J. L. Sessler, *Acc. Chem. Res.* **2012**, *45*, 1390–1401.
[35] M. Arunachalam, H. W. Gibson, *Prog. Polym. Sci.* **2014**, *39*, 1043–1073.
[36] J. Liang, S. Xing, P. Brandt, A. Nuhnen, C. Schlüsener, Y. Sun, C. Janiak, *J. Mater. Chem. A* **2020**, *8*, 19799–19804.
[37] Y. Li, S. Tang, A. Yusov, J. Rose, A. N. Borrfors, C. T. Hu, M. D. Ward, *Nat. Commun.* **2019**, *10*, 4477.
[38] B. Wang, R.-B. Lin, Z. Zhang, S. Xiang, B. Chen, *J. Am. Chem. Soc.* **2020**, *142*, 14399–14416.
[39] R.-B. Lin, Y. He, P. Li, H. Wang, W. Zhou, B. Chen, *Chem. Soc. Rev.* **2019**, *48*, 1362–1389.
[40] T. Orlando, J. De Maria Perez, F. F. S. Farias, P. R. S. Salbego, A. Martinez-Cuezva, M. A. P. Martins, J. Berna, *Cryst. Growth Des.* **2023**.
[41] P. Kuzmič, *Anal. Biochem.* **1996**, *237*, 260–273.
[42] P. Thordarson, *Chem. Soc. Rev.* **2011**, *40*, 1305–1323.
[43] D. Brynn Hibbert, P. Thordarson, *Chem. Commun.* **2016**, *52*, 12792–12805.
[44] http://supramolecular.org/, **07.06.2023**.
[45] *APEX suite of crystallographic software*, APEX 3/4, Version 2015–5.2, Version 2021–10-0, Bruker AXS Inc., Madison, Wisconsin, USA **2015, 2021**.
[46] *SAINT*, Version 8.40 A and SADABS, Version 2016/2, Bruker AXS Inc., Madison, Wisconsin, USA, **2016**.
[47] G. Sheldrick, *Acta Crystallogr. Sect. A* **2015**, *71*, 3–8.
[48] C. B. Hubschle, G. M. Sheldrick, B. Dittrich, *J. Appl. Crystallogr.* **2011**, *44*, 1281–1284.
[49] G. Sheldrick, *Acta Crystallogr. Sect. C* **2015**, *71*, 3–8.
[50] *International Tables for Crystallography*, Vol. C (Ed.: A. J. Wilson), Kluwer Academic Publishers, Dordrecht, The Netherlands, 1992, Tables 6.1.1.4 (pp. 500–502), 4.2.6.8 (pp. 219–222), 4.2.4.2 (pp. 193–199).
[51] C. F. Macrae, I. J. Bruno, J. A. Chisholm, P. R. Edgington, P. McCabe, E. Pidcock, L. Rodriguez-Monge, R. Taylor, J. van de Streek, P. A. Wood, *J. Appl. Crystallogr.* **2008**, *41*, 466–470.
[52] D. Kratzert, J. J. Holstein, I. Krossing, *J. Appl. Crystallogr.* **2015**, *48*, 933–938.
[53] D. Kratzert, I. Krossing, *J. Appl. Crystallogr.* **2018**, *51*, 928–934.
[54] R. S. Rowland, R. Taylor, *J. Phys. Chem.* **1996**, *100*, 7384–7391.
[55] M. A. Spackman, J. J. McKinnon, *CrystEngComm* **2002**, *4*, 378–392.
[56] M. A. Spackman, D. Jayatilaka, *CrystEngComm* **2009**, *11*, 19–32.

Manuscript received: May 16, 2023
Revised manuscript received: June 9, 2023
Accepted manuscript online: June 12, 2023